Materials Advances

ROYAL SOCIETY OF CHEMISTRY

COMMUNICATION

View Article Online
View Journal | View Issue

Cite this: *Mater. Adv.*, 2024, 5, 1028

Received 4th December 2023,
Accepted 27th December 2023

DOI: 10.1039/d3ma01082a

rsc.li/materials-advances

Pentatomic carbon ring conjugated nitrogen-doped nanographene†

Jinku Bai,[a] Xiao Xu,[b] Xin-Yue Wang,[a] Xin Sun,[a] Jiaqi Liang,[a] Tongling Liang [c] and Han-Yuan Gong *[a]

A π extended N-doped nanographene molecule with pentatomic carbon ring conjugation was synthesized. The molecule, 1,14-dichloro-6,9-dimethoxyquinolino[2′,3′,4:3,4]indeno[2,1,7-*ghi*] phenanthridine (1), exhibited potential as a metal cation and proton receptor with a UV-vis and fluorescence response to selected metal cations (*e.g.*, Zn^{2+}, Zr^{4+}, Ag^{+}, Cu^{2+}, or Cd^{2+}) or protons.

Over the past two decades, there has been growing interest in N-doped carbon-rich materials.[1–17] These materials exhibit excellent characteristics and a wide range of applications, including ion recognition, optical materials, electronic devices, and catalysts.[18–23] A crucial strategy for generating these materials with precise structures is bottom-up organic synthesis.[24] A potential candidate of the smallest N-doped nanographene fragments is 2,2′-bipyridine. It has shown an impressive ability to coordinate with different metal cations and also displays effective catalytic properties.[25] Nanographene molecules containing 1,10-phenanthroline were synthesized, demonstrating limited examples of hexatomic carbon ring conjugation involving the 2,2′-bipyridinyl moiety (Fig. 1a).[23,26–28] Meanwhile, non-hexatomic carbon rings in conjugated carbon structures lead to the formation of nanographene with unique topological features and distinct properties.[29,30] However, it remains difficult to examine the effect of conjugation and substituents on non-hexatomic carbon rings (such as a pentatomic carbon ring) in N-doped nanographene.

Herein, we present the compound 1,14-dichloro-6,9-dimethoxyquinolino[2′,3′,4′:3,4]indeno[2,1,7-*ghi*]phenanthridine (**1**), a N-doped nanographene derivative consisting of a pentatomic carbon ring with conjugation (Fig. 1b). When compared to the previously reported hexatomic carbon ring conjugated N-doped nanographene (*e.g.*, tetrabenzo [*b*,*de*,*gh*,*j*] [1,10]phenanthroline, **TB(phen)**), **1** has smaller ε values at 450 nm (about a quarter of **TB(phen)**'s) and larger Stokes shift (55 nm *vs.* 35 nm, respectively). Furthermore, as a result of the pentatomic carbon ring conjugation and the influence of substituents, **1** also showed various binding selectivities and/or modes with tested metal cations or protons. The results indicated that non-hexatomic ring extension and/or substituents can be employed to control carbon-rich materials.

Initially, there was an attempt to synthesize a specific hydrogen-carbon molecule, matching to **1**, without the presence of methoxy and chloride groups. However, the final product displayed significant insolubility in all solvents, rendering exact purification and further characterisation impracticable. The synthesis of **1** is presented in Scheme 1. The

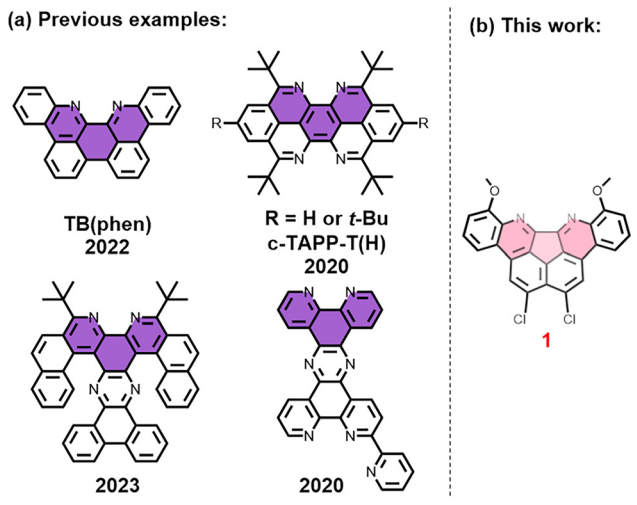

Fig. 1 (a) Previously reported hexatomic carbon ring conjugated N-doped nanographene with a core made of 2,2′-bipyridine; (b) pentatomic carbon ring conjugated 1,14-dichloro-6,9-dimethoxyquinolino [2′,3′,4′:3,4] indeno [2,1,7-*ghi*]phenanthridine (**1**) as shown in this work.

[a] College of Chemistry, Beijing Normal University, No. 19, XinJieKouWai St, HaiDian District, Beijing 100875, P. R. China. E-mail: hanyuangong@bnu.edu.cn
[b] Goods and Material Department of CASIC Tertiary Research Institute, Building 30, No. 1 Xili, Beiqu, Fengtai District, Beijing, P. R. China
[c] Institute of Chemistry, Chinese Academy of Science, Beijing 100190, P. R. China

† Electronic supplementary information (ESI) available. CCDC 2305337, 2305338 and 2305344. For ESI and crystallographic data in CIF or other electronic format see DOI: https://doi.org/10.1039/d3ma01082a

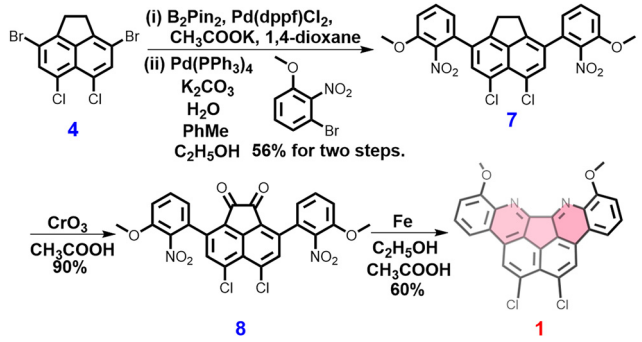

Scheme 1 The synthesis of **1**.

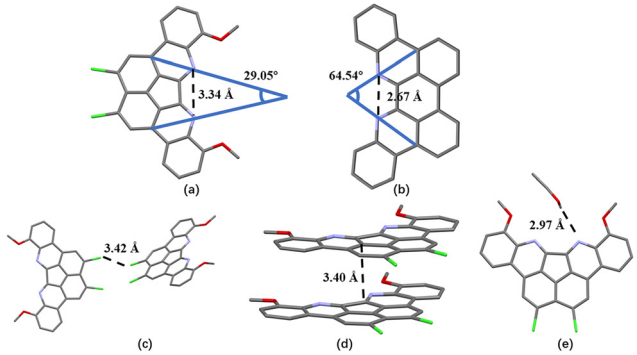

Fig. 2 **1** (a) and **TB(phen)** (b) are shown in the single crystal of [**1**·C_2H_5OH] and [**TB(phen)**·C_2H_5OH]. Colour code: C, grey; N, blue; H, white; O, red; Cl, green. (c) A representation of intermolecular halogen bonding between adjacent **1**. (d) Intermolecular π–π donor acceptor interaction between neighbour **1**. (e) The interaction between **1** and C_2H_5OH is shown.

incorporation of chlorine functional groups modifies the localization effect of subsequent bromination reaction. After undergoing boron esterification and a subsequent Suzuki coupling reaction, the compound 3,8-dibromo-5,6-dichloro-1,2-dihydroacenaphthylene (**4**)[31] was transformed into the coupling product 5,6-dichloro-3,8-bis(3-methoxy-2-nitrophenyl)-1,2-dihydro-acenaphthylene (**7**) with an overall yield of 56%. **7** was oxidized using chromium trioxide in glacial acetic acid to produce 5,6-dichloro-3,8-bis(3-methoxy-2-nitrophenyl)acenaphthylene-1,2-dione (**8**) with a yield of 90%. Ultimately, the reduction of nitro groups on **8** and carbonyl-amine condensation in one pot generated **1** with a remarkable yield of 60% using iron powder in CH_3COOH/C_2H_5OH (Scheme 1).

1 was characterized with high resolution mass spectrometry (HRMS) ($[M + H]^+$ calcd 457.0511; found: 457.0502), as well as ^1H and ^{13}C NMR spectroscopic study in $CDCl_3$ (Fig. S9, S10 and S14, ESI†). The structure of **1** was further confirmed using a single crystal X-ray diffraction analysis (Fig. S15, ESI†). The single crystal sample of **1**·C_2H_5OH was obtained by slowly evaporating a solution mixture consisting of **1** (5 mg) and 6 mL CH_2Cl_2/C_2H_5OH (2 : 1, v/v). The interatomic distance between two nitrogen atoms on 1 is 3.34 Å, representing a 25% increase compared to the distance on **TB(phen)** (2.67 Å). The angle formed with the intersection of the lines connecting the N atom and the carbon atom on the 4-site of the pyridinyl group is utilized to determine the angle of the nitrogen electron pair. The angle for **1** or **TB(phen)** is 29.05° and 64.54°, respectively (Fig. 2a and b). A neutral halogen bonding interaction between two adjacent **1** molecules occurred, with an intermolecular atomic distance of 3.42 Å (Fig. 2c). Additionally, **1** can bind to another neighbouring **1** *via* π–π donor acceptor interaction, with the intermolecular C–C atomic distance as 3.40 Å (Fig. 2d). The distance between the nitrogen atom on **1** and the oxygen atom on the C_2H_5OH is 2.97 Å. This distance means that each **1** can form a hydrogen bonding contact with an ethanol molecule (Fig. 2e).

Although **1** is not soluble in tetrahydrofuran (THF) or carbon disulfide (CS_2), it is soluble in CH_2Cl_2. In the following study, a solvent system of CH_2Cl_2/CH_3OH (4 : 1, v/v) was utilized to dissolve both the receptor (**1**) and substrates (*e.g.*, metal salts), respectively. **1** displays three distinct UV-vis absorption peaks at wavelengths of 400 nm, 425 nm, and 450 nm. These peaks correspond to molar absorptivity (ε) values of 1.12×10^4 M^{-1} cm^{-1}, 8.54×10^3 M^{-1} cm^{-1} and 8.16×10^3 M^{-1} cm^{-1}, respectively. The maximum ε values of **TB(phen)** are found under the same conditions at longer wavelengths, specifically as 1.50×10^4 M^{-1} cm^{-1} (398 nm), 2.36×10^4 M^{-1} cm^{-1} (427 nm) and 2.92×10^4 M^{-1} cm^{-1} (451 nm). Excitation at a wavelength of 400 nm in the same solvent generates a single emission peak at 505 nm (Fig. 3). The fluorescence lifetime (τ) of **1** is 3.44 ns, and the fluorescence quantum yield (Φ_F) is 0.20. The fluorescence of **TB(phen)** was measured under identical conditions, with Φ_F as 0.49, τ as 3.51 ns, and a maximum value at 515 nm (Fig. S50, ESI†).

The electrochemical properties of **1** and **TB(phen)** in CH_2Cl_2/CH_3OH (4 : 1, v/v) were evaluated using cyclic voltammetry (CV) and differential pulse voltammetry (DPV). Multistage redox behaviors were observed (Fig. 4). **1** exhibited a quasi-reversible reduction process with an $E_{1/2}$ value of −0.73 V. **TB(phen)** displayed two quasi-reversible reduction processes ($E_{1/2}^{re1} = -0.57$ V, $E_{1/2}^{re2} = -1.20$ V).

In order to gain a deeper understanding of the spectra and electrochemical differences between **1** and **TB(phen)**, density

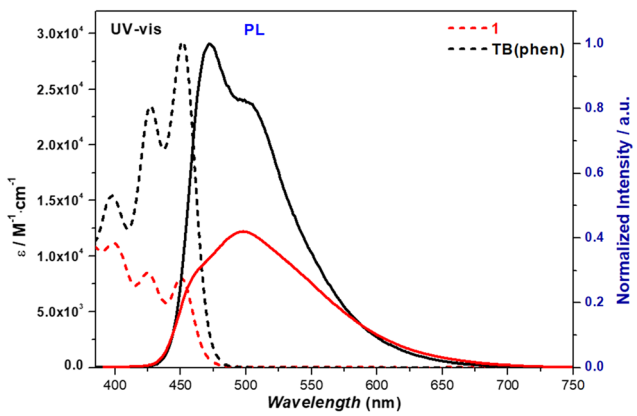

Fig. 3 UV-vis (dashed lines) and fluorescence emission spectra (solid lines) corresponding to **1** (red) and **TB(phen)** (black) (each concentration as 0.020 mM, λ_{ex} = 400 nm) in CH_2Cl_2/CH_3OH (4 : 1, v/v).

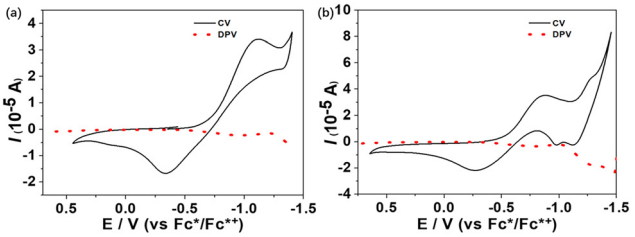

Fig. 4 CV (black solid lines) and DPV (red dashed lines) curves of **1** (a) and **TB(phen)** (b) (*vs.* Fc*/Fc*$^{+}$, Fc* = Ferrocene) in CH_2Cl_2/CH_3OH (4 : 1, v/v). Supporting electrolyte: 0.1 M Bu_4NPF_6. Working electrode: glassy carbon. Counter electrode: Pt wire. Reference electrode: Ag. Scan rate: 100 mV s^{-1}.

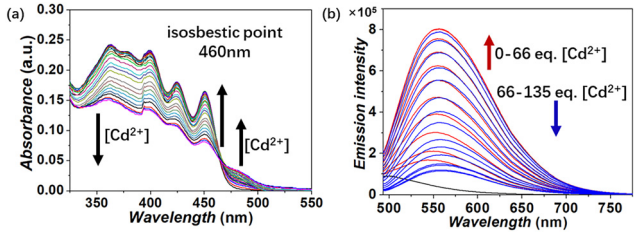

Fig. 5 UV-vis (a) and fluorescence (b) titration of **1** (2.00×10^{-5} M) with increasing Cd^{2+} in CH_2Cl_2/CH_3OH (4 : 1, v/v).

functional theory (DFT) calculations were carried out at the B3LYP/6-31G(d) level. The results suggest that the absorption peak observed at a wavelength of 450 nm can be attributed to the transition from the ground state (S_0) to the first excited state (S_1), which corresponds to the transition from the highest occupied molecular orbital (HOMO) to the lowest unoccupied molecular orbital (LUMO). The respective oscillator strength (f) values were determined to be 0.3643 and 0.6236. The incorporation of a pentatomic carbon ring conjugation and the substituents led to similar energy gap values between the HOMO and LUMO of **1** and **TB(phen)** (Fig. S71 and S72, ESI†). This is consistent with the observation that the wavelengths of their longest absorption peaks were comparable.

The UV-vis test demonstrated that compound **1** exhibits selective response towards Co^{2+}, Ni^{2+}, Cu^{2+}, Zn^{2+}, Ag^{+}, Zr^{4+} and Cd^{2+} out of the tested 32 metal cations. These metal cations include alkali, alkaline earth, transition, and lanthanide cations. All the metal cations were explored in the form of their NO_3^- salts, except for $AgBF_4$, $ZrCl_4$ and $NiCl_2$ (Fig. S20–S34, ESI†). In order to examine the specific modes of the complexation between **1** and metal cations, an initial investigation was carried out using Cd^{2+}. The spectroscopic Job plot revealed a maximum value at a molar fraction of 0.66 ([M]/[M] + [L]) (where L represents **1** and M represents Cd^{2+}). It suggested that the most stable interaction between **1** and Cd^{2+} is best described with a 1 : 2 (L/M) complexation (Fig. S33, ESI†). In the UV-vis titration, the absorbance of **1** decreased at wavelengths less than 460 nm (known as the isosbestic point) as the concentration of Cd^{2+} grew. However, a shoulder peak increased at wavelengths above 460 nm (see Fig. 5a). The association constant ($\log K_a$) was calculated *via* nonlinear fitting analysis as 6.1. The fluorescence intensity of **1** increased with the addition of Cd^{2+} in the range of 0–66 molar equiv., and then decreased in the range of 66–135 molar equiv. (Fig. 5b).

The interactions between **1** and the other tested metal cations, including Zr^{4+}, Co^{2+}, Ni^{2+}, Cu^{2+}, Zn^{2+} or Ag^{+}, were examined using comparable methods. Table 1 provided a comparison of the binding stoichiometries and association constants (expressed as $\log K_a$) for the metal cations evaluated with **1** or **TB(phen)**. When examining the complexation of Cd^{2+} as an example, it was shown that its interaction with **1** or **TB(phen)** showed significant differences in their values (6.1 *vs.* 12.3). In addition, the equilibrium ratios of **1** and **TB(phen)** with the identical metal exhibited disparity. The equations corresponding to the equilibria, which have been calculated using the most accurate non-curve fitting method, are provided below:

$$aL + bM \overset{K}{\rightleftharpoons} M_bL_a \quad K = \frac{L_aM_b}{[L]^a[M]^b}$$

The interaction between **1** and metal cations was verified using electrospray ionization high resolution mass spectrometric (ESI-HRMS) analysis (Fig. S59–S63, ESI†). This indicates that the binding is also chemically stable in the gas phase.

To gain deeper insight into the coordination modes between **1** and metal cations, single crystal X-ray diffraction analysis of $[\mathbf{1}\cdot Zn^{2+}]\cdot(NO_3^-)_2\cdot CH_3OH$ and $[\mathbf{1}\cdot Cd^{2+}]\cdot(NO_3^-)_2\cdot 2CH_3OH$ was carried out (Fig. 6d and e). After dissolving **1** (2 mg) and 25 molar equiv. of $Zn(NO_3)_2\cdot 6H_2O$ or 20 molar equiv. of $Cd(NO_3)_2\cdot 4H_2O$ in a mixed solvent of 4 mL $ClCH_2CH_2Cl/CH_3OH$ (1 : 1, v/v), red needle-shaped single crystal samples of $[\mathbf{1}\cdot Zn^{2+}]\cdot(NO_3^-)_2\cdot CH_3OH$ or $[\mathbf{1}\cdot Cd^{2+}]\cdot(NO_3^-)_2\cdot 2CH_3OH$ were grown through gradual evaporation. Zinc and cadmium, although they are in the same group, have different coordination numbers of 6 and 8, respectively, in **1** complexation. This discrepancy emerges due to their distinct atomic sizes (Fig. 6a and b). Both complexes demonstrated metal coordination with a single nitrogen atom and an adjacent oxygen atom on **1**. In order to investigate the various binding modes between **1** or **TB(phen)** and Cd^{2+}, the two complex structures were compared. The Cd^{2+} ion in the crystal formed a 1 : 1 combination with **1**. In addition, the Cd^{2+} ion displayed octacoordination, with two methanol molecules, two nitrate anions, and one nitrogen and one neighboring oxygen atom on **1** surrounding it. The crystal structure of $[\mathbf{TB(phen)}\cdot Cd^{2+}\cdot(NO_3^-)_2]\cdot CH_3OH$, as previously described, revealed a coordination number of 7 for Cd^{2+}. In this case, Cd^{2+} formed a complex with four oxygen atoms from nitrate anions, two nitrogen atoms from **TB(phen)**, and one oxygen atom from methanol (Fig. 6c and f). Unlike the **TB(phen)** complex, the **1** complex has only one nitrogen atom that can coordinate with a single Cd^{2+} ion. The results may be due to the relationship between the longer N–N distance, the lower electron pair angle, and the substituent effect.

The investigation focused on the complexation process between **1** or **TB(phen)** and Cd^{2+} ions, characterized by the pseudoequilibrium (Scheme 2). Theoretical calculations were performed separately using either the MM+ force field or the

Table 1 Summary of the interactions between **1** or **TB(phen)** and metal cations in CH_2Cl_2/CH_3OH (4 : 1, v/v)

Metal cations	**1** [M] : [L]	log K_a UV-vis	**TB(phen)** [M] : [L]	log K_a UV-vis	Metal cations	**1** [M] : [L]	log K_a UV-vis	**TB(phen)** [M] : [L]	log K_a UV-vis
Co^{2+}	2 : 1	5.5(3)	2 : 1	12.3(3)	Zn^{2+}			3 : 2	23.6(4)
			1 : 1	6.3(6)	Zr^{4+}	1 : 1	4.1(2)	1 : 1	11.7(5)
			3 : 2	23.9(2)				1 : 2	16.5(5)
Ni^{2+}	1 : 1	3.7(2)	1 : 1	6.8(3)				2 : 1	16.9(8)
			3 : 2	23.5(2)	Ag^{+}	1 : 1	3.6(2)	1 : 1	6.8(6)
			2 : 1	12.5(3)				1 : 2	12.6(3)
Cu^{2+}	1 : 1	3.3(2)	1 : 1	8.9(3)				3 : 3	24.6(3)
			1 : 2	16.2(2)	Cd^{2+}	2 : 1	6.1(3)	2 : 1	12.3(5)
Zn^{2+}	1 : 1	3.2(2)	1 : 1	6.3(5)				1 : 1	7.3(2)
			2 : 1	11.9(2)				3 : 2	24.9(4)

Only the association constant (log K_a) of the most thermostable complex of **1** was calculated due to the weak and complicated interaction (including possible solvent competition and/or the other complexations, *etc.*).

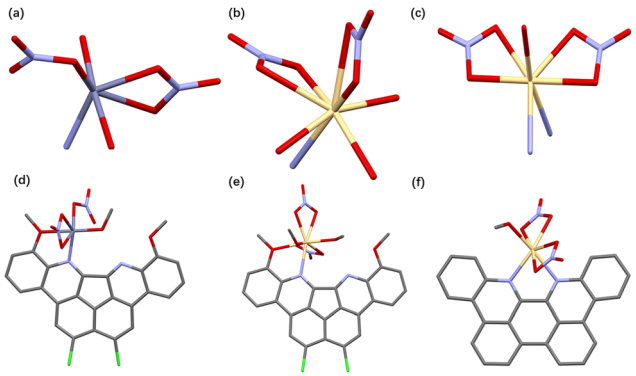

Fig. 6 The binding modes between **1** and Zn^{2+}, as well as **1** or **TB(phen)** and Cd^{2+} in the single crystal structure of [**1**·Zn^{2+}]·$(NO_3^-)_2$·CH_3OH (a) and (d), [**1**·Cd^{2+}]·$(NO_3^-)_2$·$2CH_3OH$ (b) and (e) or [**TB(phen)**·Cd^{2+}·$(NO_3^-)_2$]·CH_3OH (c) and (f). Colour code: C, grey; N, blue; O, red; Cl, green; Zn, purple: Cd, yellow.

PM7 method, in either a vacuum or aqueous environment. The findings were in agreement with the experimental results. More precisely, when the ratio of L to M is 1 : 1, the **TB(phen)** complex shows a stronger interaction compared to **1**'s. When the ratio of L to M is 2 : 1, they display similar powerful interactions. When the ratio of L to M is 1 : 2, it is observed that only the complex of **1** can exist in a stable manner (Table 2).

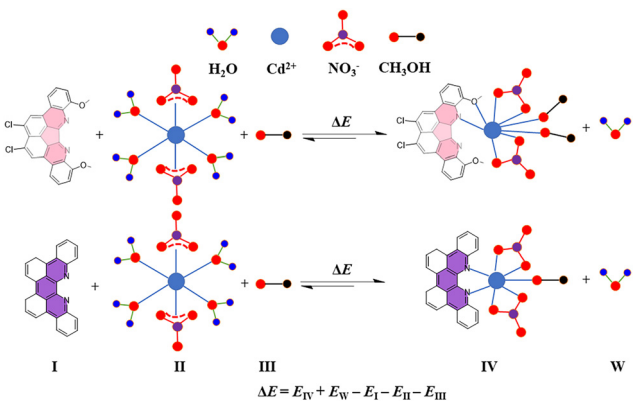

Scheme 2 Scheme presentation of the complexation equilibriums between $Cd(NO_3)_2$·$4H_2O$ and **1** or **TB(phen)** with a 1 : 1 ratio.

The proton sensitivity of **1** was further investigated *via* carefully monitoring the changes in UV-vis or fluorescence spectra as the trifluoromethanesulfonic acid (TfOH) concentration increased (Fig. S79 and S80, ESI†). Specifically, the UV-vis spectra of compound **1** (2.00×10^{-5} M in CH_2Cl_2/CH_3OH (4 : 1, v/v)) exhibited a drop in intensity with wavelength shorter than 462 nm (*i.e.*, the isosbestic point). Additionally, a new broad absorption band with two distinct peaks at 515 and 550 nm was seen. **1** has an emission peak at 630 nm with the excitation wavelength at 540 nm. Φ_F of the mixture containing **1** and 20 molar equiv. of TfOH was 5.8%, and τ was 1.78 ns.

In conclusion, we have described a N-doped nanographene derivative **1** as a π extended 2,2′-bipyridine, featuring a conjugation of a pentatomic carbon ring. Experimental and theoretical calculations indicated that including a pentatomic carbon ring with a conjugated structure, combined with the influence of substituents, led to substantial modifications in the overall skeleton structure. The modifications include the distribution of nitrogen atoms and the angle between electron pairs. Subsequently, the molecule can display distinctive characteristics when it interacts with metal cations or protons, as opposed to the hexatomic carbon ring conjugated **TB(phen)**. This implies that involving a conjugated system with a non-hexatomic carbon ring can effectively regulate the structure and properties of N-doped nanographene molecules.

Prof. H.-Y. Gong is grateful to the National Natural Science Foundation of China (92156009 and 21971022), the Fundamental Research Funds for the Central Universities, the Beijing

Table 2 Energy difference (kcal mol^{-1}) of the complexation between Cd^{2+} and the ligand

		ΔE (L : Cd^{2+})		
Method[a]	Ligand	1 : 2	1 : 1	2 : 1
MM+	**1**	2.26	4.81	−12.92
	TB(phen)	[b]	−7.53	14.03
PM7	**1**	−187.19	−113.35	−233.68
	TB(phen)	[b]	−274.52	−216.18

[a] Molecular mechanics (MM+) under vacuum and PM7 in water. Solvation is accounted for by applying a 1.65 nm × 1.65 nm × 1.65 nm periodic box. [b] The complex exhibits excessive instability and the structure optimization is unsuccessful.

Municipal Commission of Education, and Beijing Normal University for financial support. Dr J. Bai is grateful to Dr S. Wang for the theoretical calculation.

Conflicts of interest

There are no conflicts to declare.

Notes and references

1 Y. Zhang, S. H. Pun and Q. Miao, *Chem. Rev.*, 2022, **122**, 14554.
2 S. Yang, M. Chu and Q. Miao, *J. Mater. Chem. C*, 2018, **6**, 3651.
3 Y.-M. Liu, Y.-Q. Huang, S.-H. Liu, D. Chen, C. Tang, Z.-L. Qiu, J. Zhu and Y.-Z. Tan, *Angew. Chem., Int. Ed.*, 2019, **58**, 13276.
4 R. Gao, Z. Liu, Z. Liu, T. Liang, J. Su and L. Gan, *Angew. Chem., Int. Ed.*, 2023, **62**, e202300151.
5 S. Sun, Z. Liu, F. Colombo, R. Gao, Y. Yu, Y. Qiu, J. Su and L. Gan, *Angew. Chem., Int. Ed.*, 2022, **61**, e202212090.
6 M. Wang, H. Shi, P. Zhang, Z. Liao, M. Wang, H. Zhong, F. Schwotzer, A. S. Nia, E. Zschech, S. Zhou, S. Kaskel, R. Dong and X. Feng, *Adv. Funct. Mater.*, 2020, **30**, 2002664.
7 G. Wang, N. Chandrasekhar, B. P. Biswal, D. Becker, S. Paasch, E. Brunner, M. Addicoat, M. Yu, R. Berger and X. Feng, *Adv. Mater.*, 2019, **31**, 1901478.
8 Y. Fu, H. Yang, Y. Gao, L. Huang, R. Berger, J. Liu, H. Lu, Z. Cheng, S. Du, H.-J. Gao and X. Feng, *Angew. Chem., Int. Ed.*, 2020, **59**, 8873.
9 F. C. Parks, E. G. Sheetz, S. R. Stutsman, A. Lutolli, S. Debnath, K. Raghavachari and A. H. Flood, *J. Am. Chem. Soc.*, 2022, **144**, 1274.
10 W. Zhao, J. Tropp, B. Qiao, M. Pink, J. D. Azoulay and A. H. Flood, *J. Am. Chem. Soc.*, 2020, **142**, 2579.
11 G. Li, T. Matsuno, Y. Han, H. Phan, S. Wu, Q. Jiang, Y. Zou, H. Isobe and J. Wu, *Angew. Chem., Int. Ed.*, 2020, **59**, 9727.
12 J. Zhu, S. Wu, X. Hou and J. Wu, *Angew. Chem., Int. Ed.*, 2021, **60**, 25323.
13 W. Zhou, T. Sarma, L. Yang, C. Lei and J. L. Sessler, *Chem. Sci.*, 2022, **13**, 7276.
14 X. Guo, Z. Yuan, Y. Zhu, Z. Li, R. Huang, Z. Xia, W. Zhang, Y. Li and J. Wang, *Angew. Chem., Int. Ed.*, 2019, **58**, 16966.
15 W.-W. Zhang, Q. Wang, S.-Z. Zhang, C. Zheng and S.-L. You, *Angew. Chem., Int. Ed.*, 2023, **62**, e202214460.
16 Q. Wang, W.-W. Zhang, C. Zheng, Q. Gu and S.-L. You, *J. Am. Chem. Soc.*, 2021, **143**, 114.
17 Y. Wang, X.-S. Ke, S. Lee, S. Kang, V. M. Lynch, D. Kim and J. L. Sessler, *J. Am. Chem. Soc.*, 2022, **144**, 9212.
18 X.-Y. Wang, X. Yao, A. Narita and K. Müllen, *Acc. Chem. Res.*, 2019, **52**, 2491.
19 Y.-M. Liu, H. Hou, Y.-Z. Zhou, X.-J. Zhao, C. Tang, Y.-Z. Tan and K. Müllen, *Nat. Commun.*, 2018, **9**, 1901.
20 A. Narita, X.-Y. Wang, X. Feng and K. Müllen, *Chem. Soc. Rev.*, 2015, **44**, 6616.
21 D. Guo, R. Shibuya, C. Akiba, S. Saji, T. Kondo and J. Nakamura, *Science*, 2016, **351**, 361.
22 H. Yin, C. Zhang, F. Liu and Y. Hou, *Adv. Funct. Mater.*, 2014, **24**, 2930.
23 X. Xu, T. Xia, X.-L. Chen, X. Hao, T. Liang, H.-R. Li and H.-Y. Gong, *New J. Chem.*, 2022, **46**, 11835.
24 L. Zhou, B. Wu, Y. Chen, J. Gong, J. Wang, G. Dai, C. Chi and Q. Wang, *Org. Lett.*, 2021, **23**, 8640.
25 S. Banerjee, B. Senthilkumar and N. T. Patil, *Org. Lett.*, 2019, **21**, 180.
26 W. Yuan, J. Cheng, X. Li, M. Wu, Y. Han, C. Yan, G. Zou, K. Müllen and Y. Chen, *Angew. Chem., Int. Ed.*, 2020, **59**, 9940.
27 Z. Yu, G. Shi, K.-P. Wang, L.-Z. Xu, S. Chen and Z.-Q. Hu, *Tetrahedron*, 2023, **130**, 133178.
28 R. Zibaseresht, *Synth. Commun.*, 2020, **50**, 904.
29 C. Wang, Z. Deng, D. L. Phillips and J. Liu, *Angew. Chem., Int. Ed.*, 2023, **62**, e202306890.
30 H. Luo and J. Liu, *Angew. Chem., Int. Ed.*, 2023, **62**, e202302761.
31 Y. Fei, Y. Fu, X. Bai, L. Du, Z. Li, H. Komber, K.-H. Low, S. Zhou, D. L. Phillips, X. Feng and J. Liu, *J. Am. Chem. Soc.*, 2021, **143**, 2353.